HiSST: 3rd International Conference on
High-Speed Vehicle Science Technology
14 -19 April 2024, Busan, Korea

Numerical Study on Unstart Characteristics of Scramjet Engine Induced by Fuel Injection

Hyunwoo Kim[1], Hong-Gye Sung[2]

Abstract

The unstart phenomenon in a scramjet engine was simulated using fuel injection. Unstart conditions were tested under two different flight conditions, light Mach number and angle of attack. To simulate the unstart process, an analysis of the unsteady flow within the flow path of the engine was conducted using a Hybrid RANS/LES turbulence model incorporating compressibility and low Reynolds number corrections. The presence of unstart induced by fuel flow rates was analyzed using the Korkegi criterion. For quantitative analysis, the pressure distributions at specific wall pressure sensors were examined. The CUSUM algorithm was utilized to identify the initiation of unstart, revealing a delayed onset of unstart with increasing angle of attack.

Keywords : *unstart, fuel injection, hybrid RANS/LES, CUSUM Algorithm.*

Nomenclature

D – Diffusion coefficient
E – Total energy
H(t) – Heaviside function
h – Static enthalpy
k – Turbulent kinetic energy
p – Static pressure
Pr – Prandtl number
ρ – Density
Sc – Schmidt number
t – Time
u – Velocity
Y – Species mass fraction

Greek
δ_{ij} – Kronecker delta
μ – Molecular viscosity
τ_{ij} – Shear stress
ω – Specific dissipation rate

Superscripts
$\bar{}$ – Time averaged
$\tilde{}$ – Favre averaged
$''$ – Fluctuation

Subscripts
i, j, k – Spatial coordinate index
t – Turbulent

1. Introduction

Scramjet engines, capable of hypersonic flight, remain a subject of extensive research. As the flow encounters the isolator, it forms a shock train, minimizing flow disturbances while compressing as it enters the combustion chamber. The stability of the shock train is crucial, but various factors such as changes in flight conditions, mode transitions, fuel injection, and combustion instability can lead to the complex phenomenon of shock-wave boundary layer interaction. Consequently, instability in the shock system can cause flow separation and result in unstart, leading to a rapid decrease in thrust. Notably,

[1]*Korea Aerospace University, 76 Hanggongdaehak-ro Deogyang-gu Goyang-si Gyeonggi-do, hyunwoo5316@kau.kr*
[2]*Korea Aerospace University, 76 Hanggongdaehak-ro Deogyang-gu Goyang-si Gyeonggi-do, hgsung@kau.ac.kr*

the failed flight test of the NASA X-51A scramjet engine underscores the importance of studying and predicting unstart characteristics [1].

However, due to the complex physical phenomena and unsteady characteristics of unstart, research is primarily conducted through ground experiments. Mashio et al. conducted experiments on the characteristics of unstart induced by excessive heat release, confirming the discontinuity of unstart transition when injecting fuels with high equivalence ratios [2]. Wagner et al. investigated the time-dependent characteristics of the unstart shock system through mechanical throttling in low enthalpy flows [3]. Do et al. studied the characteristics of boundary layers in unstart induced by mass injection [4] and Im et al. conducted research on the unstart process induced by mass addition and heat release in both low and high enthalpy flows, confirming variations in unstart characteristics depending on the incoming air properties [5]. Baccarella et al. analyzed the behavior of shock trains when unstart occurs in low enthalpy flows using Rayleigh scattering imaging [6]. As seen in the above research cases, experiments with scaled-down models are predominantly conducted.

In this study, unstart in an scramjet engine is simulated through fuel injection. Additional analysis is conducted on variations in angle of attack and Mach number to confirm unstart characteristics under different flight conditions. A Hybrid RANS/LES model is applied to simulate unsteady flow, and dynamic pressure patterns obtained during the unstart process are analyzed. The presence of unstart is determined using the Korkegi criterion [7]. Additionally, the CUSUM algorithm [8-10] is applied to predict the detection of unstart.

2. Numerical Method

2.1. Governing equation

The governing equations for the three-dimensional, time-dependent, non-reacting and Favre-averaged compressible equations are as follows:

$$\frac{\partial \bar{\rho}}{\partial t} + \frac{\partial \bar{\rho}\widetilde{u_j}}{\partial x_j} = 0 \tag{1}$$

$$\frac{\partial \bar{\rho}\widetilde{u_i}}{\partial t} + \frac{\partial \bar{\rho}\widetilde{u_i}\widetilde{u_j}}{\partial x_j} + \frac{\partial \bar{p}}{\partial x_i} = \frac{\partial}{\partial x_j}\left(\overline{\tau_{ij}} - \overline{\rho u_i'' u_j''}\right) \tag{2}$$

$$\frac{\partial \bar{\rho}\tilde{E}}{\partial t} + \frac{\partial\left(\left(\bar{\rho}\tilde{E} + \bar{p}\right)\widetilde{u_j}\right)}{\partial x_j} = \frac{\partial}{\partial x_j}\left[\left(\overline{\tau_{ij}} - \overline{\rho u_i'' u_j''}\right)\widetilde{u_i}\right] - \frac{\partial}{\partial x_j}\left(\bar{q}_j + \overline{\rho u_j'' h''}\right) + \frac{\partial}{\partial x_j}\left[-\frac{1}{2}\overline{\rho u_i'' u_j'' u_j''} + \overline{\tau_{ij} u_i''}\right] \tag{3}$$

$$\frac{\partial \bar{\rho}\widetilde{Y_i}}{\partial t} + \frac{\partial \bar{\rho}\,\widetilde{Y_i}\widetilde{u_j}}{\partial x_j} = \frac{\partial}{\partial x_j}\left(\bar{\rho}D_i\frac{\partial \tilde{Y}_i}{\partial x_j} - \overline{\rho Y_i'' u_j''}\right) \tag{4}$$

Where p is the static pressure, u_i is the velocity in the i-direction, E is the total energy, Y is the mass fraction of species and k is the turbulent kinetic energy. The superscripts '$\bar{}$' and '$\tilde{}$' denote Reynolds and Favre averaging, respectively. ρ, h, τ_{ij} and D_i are the density, enthalpy, shear stress and diffusion coefficients of species, respectively. $-\overline{\rho u_i'' u_j''}$ represents the Reynolds stress tensor. Using the Boussinesq approximation, the sum of molecular stress and Reynolds stress tensor can be expressed as follows:

$$\overline{\tau_{ij}} - \overline{\rho u_i'' u_j''} = (\mu + \mu_t)\left(\frac{\partial \tilde{u}_i}{\partial x_j} + \frac{\partial \tilde{u}_j}{\partial x_i} - \frac{2}{3}\delta_{ij}\frac{\partial \tilde{u}_k}{\partial x_k}\right) - \frac{2}{3}\bar{\rho}k\delta_{ij} \tag{5}$$

Similarly, additional terms are expressed through closure hypothesis as follows:

$$-\overline{\rho u_j'' h''} = \frac{\mu_t}{Pr_t}\frac{\partial \tilde{h}}{\partial x_j} \tag{6}$$

$$-\frac{1}{2}\overline{\rho u_i'' u_j'' u_j''} + \overline{\tau_{ij} u_i''} = (\bar{\mu} + \sigma_k \mu_t)\frac{\partial k}{\partial x_k} \tag{7}$$

$$-\overline{\rho Y_i'' u_j''} = \frac{\mu_t}{Sc_t}\frac{\partial \tilde{Y}_i}{\partial x_j} \tag{8}$$

where Pr_t and Sc_t are the turbulent Prandtl number and turbulent Schmidt number, respectively, each having values of 0.9 and 0.7, respectively.

2.2. Turbulent Model

The k-ω SST model, belonging to the RANS family, was developed to incorporate turbulence effects in subsonic flows [11]. However, it tends to overestimate shear stresses and predict excessive thickness of the boundary layer that develops from the laminar region in low-speed flows such as in the laminar and transitional regions. To address this issue, the compressibility correction of Wilcox [12] and the low Mach Reynolds correction of Peng [13] were applied. Additionally, RANS models have difficulties in representing unsteady motions such as detached flows due to their model based on time-averaging. On the other hand, LES models require a large number of grids, which leads to longer computational times. To overcome the limitations, the present study applied the Hybrid RANS-LES model. The equations for the IDDES model [14], which combine the compressibility correction based on the k- ω SST model and low Reynolds correction, are as follows.

$$\frac{\partial(\bar{\rho}k)}{\partial t} + \frac{\partial(\bar{\rho}\tilde{u_j}k)}{\partial x_j} = P_k - D_k\left[\beta^*{}_\infty\left(1 + \zeta^* F(M_t)\right)\left(\frac{4/15 + \left(Re_t/R_\beta\right)^4}{1 + \left(Re_t/R_\beta\right)^4}\right)\right] + \frac{\partial}{\partial x_j}\left[(\mu + \sigma_k \mu_t)\frac{\partial k}{\partial x_j}\right] \tag{9}$$

$$\frac{\partial(\bar{\rho}\omega)}{\partial t} + \frac{\partial(\bar{\rho}\tilde{u_j}\omega)}{\partial x_j} = \frac{\gamma}{\upsilon_t}P_k - \left[\beta_\infty - \beta^*{}_\infty \zeta^* F(M_t)\left(\frac{4/15 + \left(Re_t/R_\beta\right)^4}{1 + \left(Re_t/R_\beta\right)^4}\right)\right]\rho\omega^2 + \frac{\partial}{\partial x_j}\left[(\mu + \sigma_k \mu_t)\frac{\partial k}{\partial x_j}\right] \tag{10}$$

where P_k and D_k are the turbulence kinetic energy production term and the destruction term of kinetic energy, respectively. The terms for this are expressed as follows:

$$P_k = \min\left(\tau_{ij}\frac{\partial \tilde{u}_i}{\partial x_j}, 10\beta^*\rho k\omega\right) \tag{11}$$

$$D_k = \frac{\rho\sqrt{k^3}}{l_{IDDES}} \tag{12}$$

The closure coefficient and functions for compressible corrections and the Mach Reynolds corrections are defined as follows.

$$\zeta^* = 1.5, R_\beta = 8.0 \tag{13}$$

$$F(M_t) = \left[{M_t}^2 - {M_{t0}}^2\right]H(M_t - M_{t0}) \tag{14}$$

Additional variables are expressed through a blending function.

2.3. Numerical Scheme

In this study, a numerical analysis is conducted using a three-dimensional unstructured grid based in-house code. For time discretization, the preconditioned dual time steeping method is applied [15]. The convective flux is applied using the High Resolution Simple Low-dissipation AUSM2 (HR-SLAU2) scheme [16], while the viscous flux is calculated using the central difference scheme. To improve numerical stability on unstructured grids, a non-orthogonal minimum correction scheme is applied [17]. To enhance accuracy at cell interfaces, a normalized variable formulation (NVF) based Van-LEER limiter is used [17]. To minimize errors in gradients on unstructured grids, an MLP[18] limiter is additionally utilized. To enhance computational efficiency, the computational domain is divided into multiple blocks, and the Massage Passing Interface (MPI) parallel computing technique is utilized for inter-block communication.

3. Validation

To simulate the unstart process induced by fuel injection, validations are conducted against the experimental results of Im [5]. The analysis domain and boundary conditions are consistent with Fig. 1 and Table 1. The grid consisted of approximately 230,000 cells, configured to satisfy y+ ~ 1, and a two-dimension computational analysis is performed. The experimental and simulated wall pressure distributions before fuel injection along the lower wall of the internal duct are shown in Fig. 2. Although the pressure values at S2 and S3 are slightly lower than the experimental values, they follow the overall trend of the wall pressure distribution. Fig. 3 presents a comparison between the Schlieren image of the unstart process induced by nitrogen fuel injection and the Density Gradient contour of analysis results. It reveals a tendency for the analysis results to somewhat overpredict unstart compared to the experimental result. To confirm this, the Korkegi Criterion is compared using the pressure measurements at S1 and S2, resulting in a value of 4.18, which exceed the threshold of 3.7. Despite the excessive prediction of unstart compared to the experiment, the analysis shows a similar trend in the unstart process.

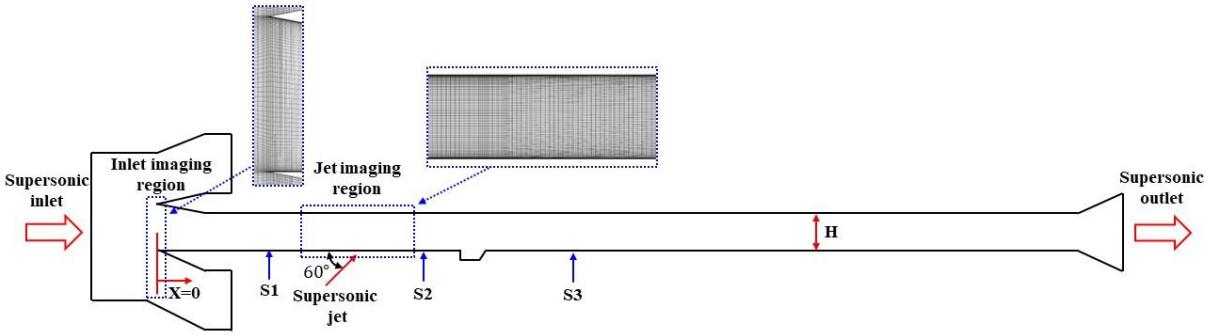

Fig 1. Computation domain

Table 1. Boundary conditions

Free stream				Jet			
P(kPa)	T(K)	M	$\dot{m}_{inflow}(g/s)$	Fuel	$\dot{m}_{jet}(g/s)$	J	$\dot{m}_{jet}/\dot{m}_{inflow}$ (%)
0.52	57.0	4.5	16.6	N_2	2.41	2.41	14.59

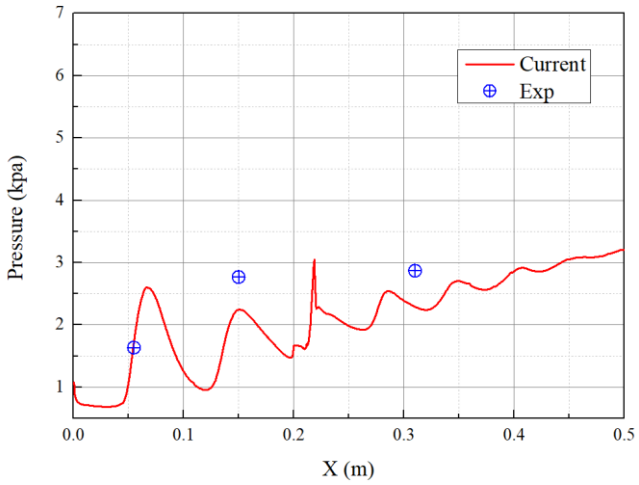

Fig 2. Comparison of pressure distributions between experimental data [5] and analysis results.

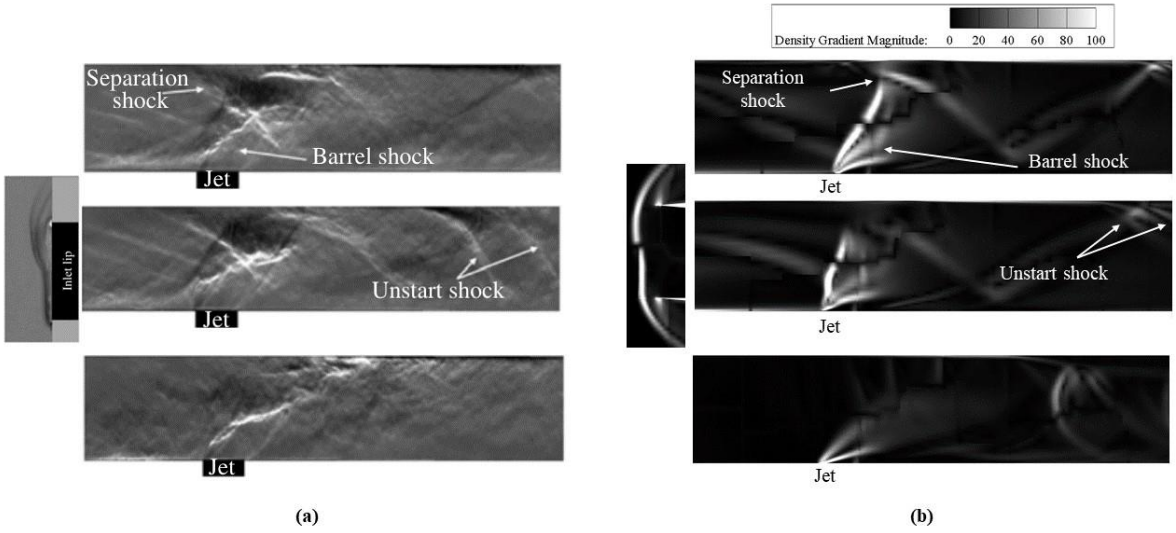

Fig 3. Comparison results of Schlieren images for the unstart flow: (a) Experimental [5] and (b) Analysis results.

4. Numerical result

4.1. Model description

In this study, the inlet-isolator-combustor model of scramjet used in previous research [19] is simulated. The computation domain is depicted in Fig. 4. A two-dimensional hybrid grid is constructed, with wall grid sizes set to Y+~5. A total of 320,000 grids are used. The origin is set at the leading edge of the inlet, and the isolator height is normalized with respect to the axial position. Air properties at an altitude of 22 km are used for flow conditions. Detailed information regarding this is presented in Table 2. The locations of pressure sensors and injectors are provided in Table 3.

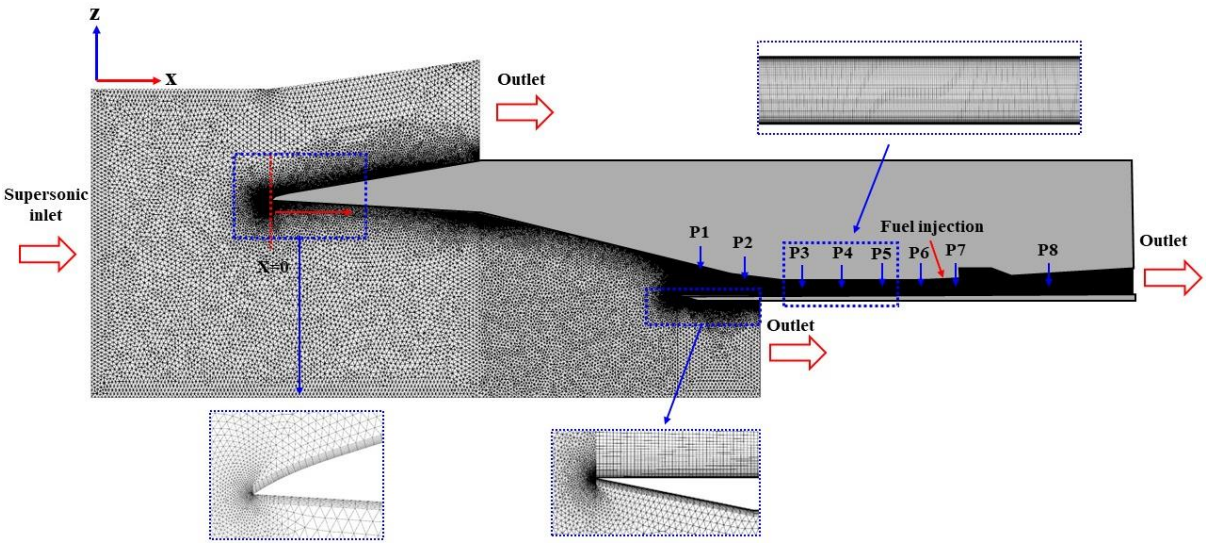

Fig 4. Computation domain

Table 2. Boundary conditions

Free stream				Fuel		
P(kPa)	**T(K)**	**M**	**AOA**	**Fuel**	**P(kPa)**	**T(K)**
4.042	218.57	5.1/5.2/5.3	-4/0/4	C_2H_4	202.65	293.0

Table 3. The locations of pressure sensor and injector

	P_1	P_2	P_3	P_4	P_5	P_6	P_7	P_8	Injector
$X(x/H)$	32.59	34.46	38.86	41.03	44.19	46.33	48.0	54.65	46.68

4.2. Unstart process

To simulate the unstart process, ethylene fuel is injected vertically, and it is observed that unstart occurred when the fuel mass flow rate exceeds 30% of the airflow. To assess the intensity of unstart, the Korkegi criterion is applied, yielding a value slightly higher than the reference value of 2.7, specifically 2.857, indicating a threshold for induced shock-induced boundary separation. This is considered as the limit of unstart, prompting further computational analysis. Fig 5. shows the unstart process using density gradient contours. At 0.3 *ms*, strong bow shock appears due to immediate fuel injection, leading to boundary layer separation at the lower wall of the internal duct due to bow shock reflection. At 1.5 *ms*, an adverse pressure gradient emerges due to shock-induced boundary separation, causing thickening of the boundary layer downstream. The thickened boundary layer results in additional induced shock. At 3.6 *ms*, as the boundary layer thickens further, a strong adverse pressure gradient leads to the occurrence of unstart shock, causing the shock train formed in the duct to move upstream. The low velocities are subsequently observed within the internally duct as shocks gradually exit the duct.

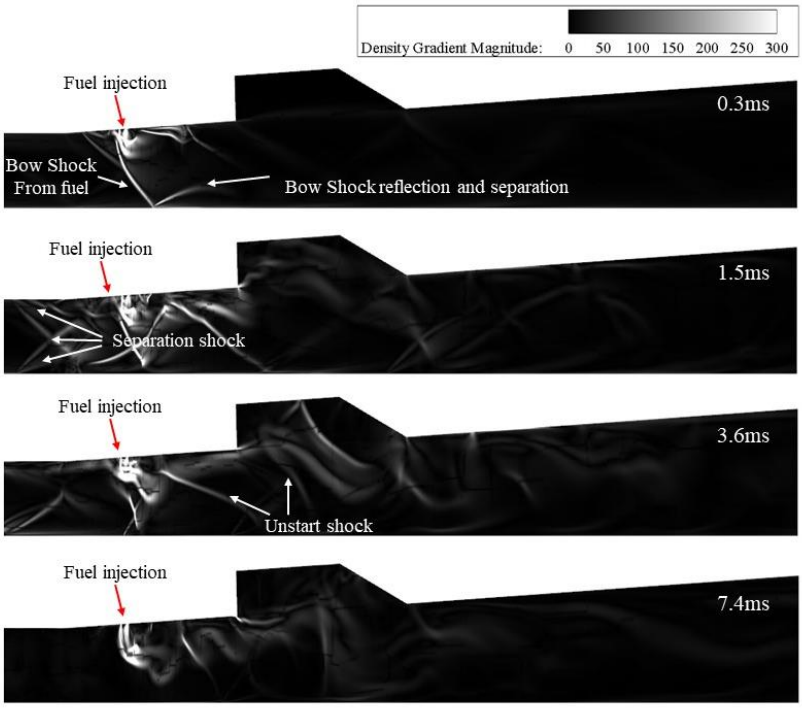

Fig 5. Density gradient contours for the unstart process at Mach 5.2 and angle of attack 0 degree

To understand the unstart characteristics under varying flight conditions, the simulations of the unstart process are conducted with variations in Mach number and angle of attack. Fig 6. shows the internal flow structure through Mach contour results, depicting changes in angle of attack and Mach number. An increase in angle of attack led to a delay in boundary layer separation. This trend emerges as the intensity of shock waves formed within the internal duct decreases with increasing angle of attack, consequently reducing the adverse pressure gradient at the boundary layer and delaying unstart. Regarding Mach number, both increases and decreases result in unstart delay.

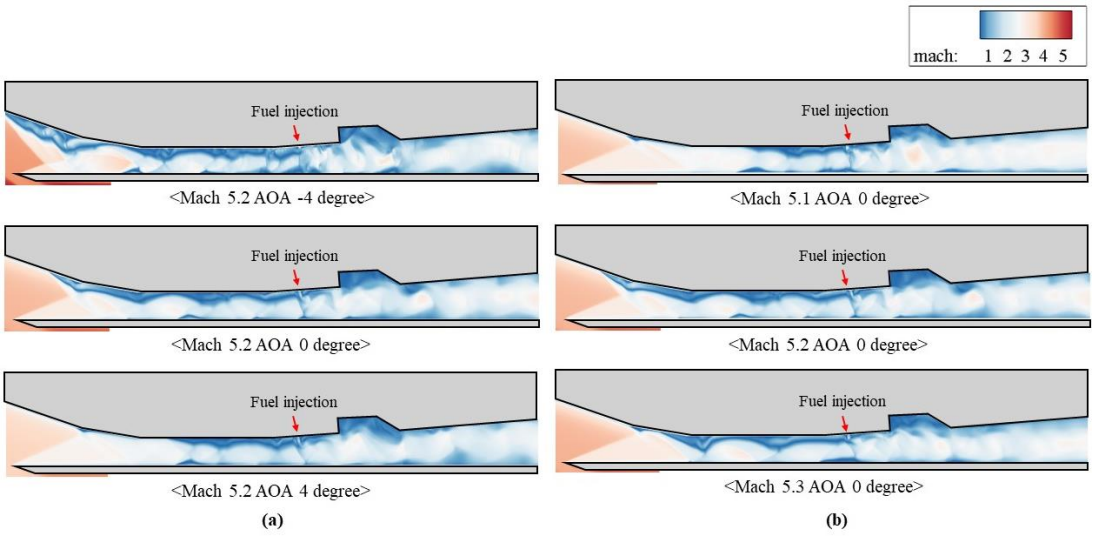

Fig 6. Mach contours at 4.0ms for variation flight conditions: angle of attack(a) and Mach number(b)

4.3. Unstart detection

Using the pressure time history measured by sensors, determining the exact moment of unstart shock arrival time poses difficulty. The coexistence of the Ram mode Shock system and unstart shock system makes it difficult to accurately identify the timing of unstart shock arrival as depicted in Fig. 7. To address this, the CUSUM algorithm is applied to detect the arrival time of unstart shock. Figs. 8 and 9 show the results of detecting the time of unstart shock arrival based on the measured pressure data from sensor P3, with variations in Mach number and angle of attack. For Mach number 5.2 and angles of attack -4°, 0°, and 4°, the arrival times of unstart are detected at 4.04 *ms*, 5.11 *ms*, and 6.83 ms, respectively. This quantitatively confirms that unstart shock advances more rapidly with lower angles of attack. At an angle of attack of 0°, arrival times of unstart for Mach numbers 5.1, 5.2, and 5.3 are detected at 7.08 *ms*, 5.11 *ms*, and 5.65 *ms*, respectively. The unstart is delayed with variations in Mach number.

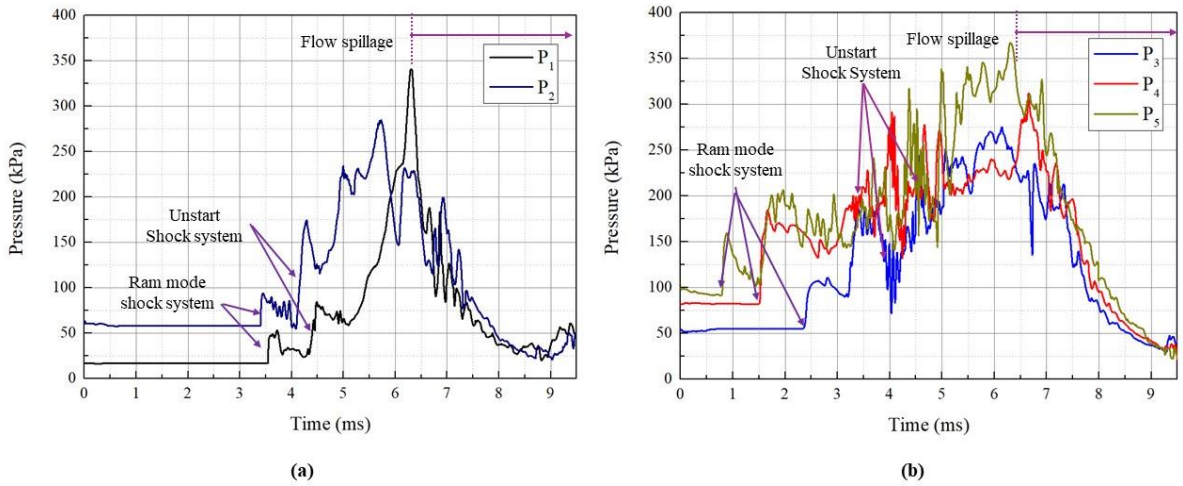

Fig 7. Pressure time history at sensors for Mach 5.2 and an angle of attack of 0 degrees: (a) P1, P2 and (b) P3, P4, P5.

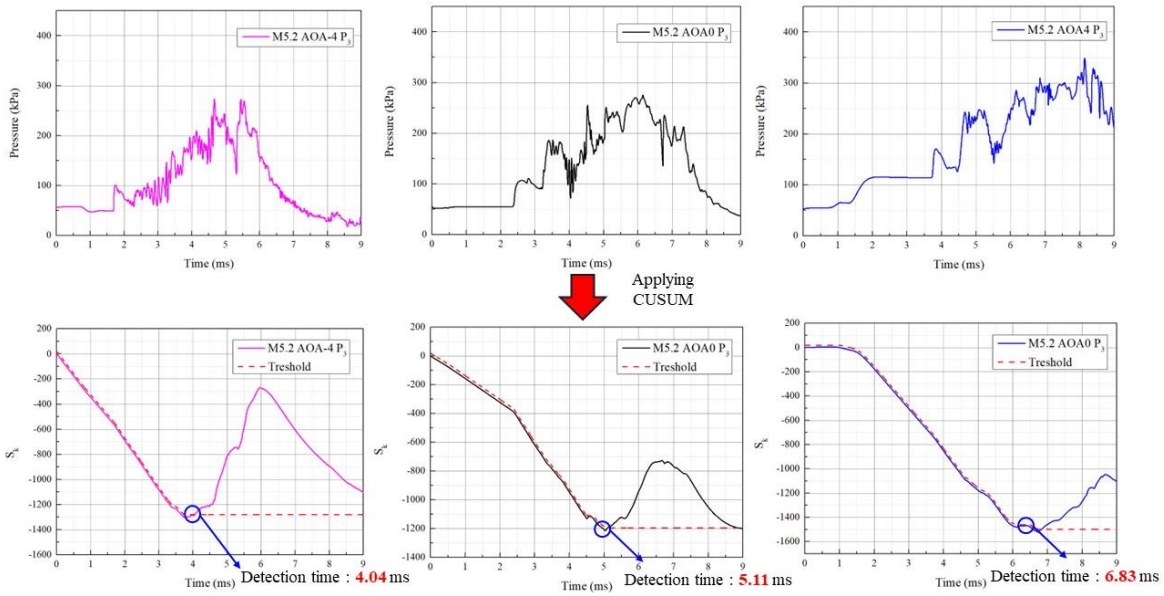

Fig 8. CUSUM algorithm for P3 sensor at Mach 5.2

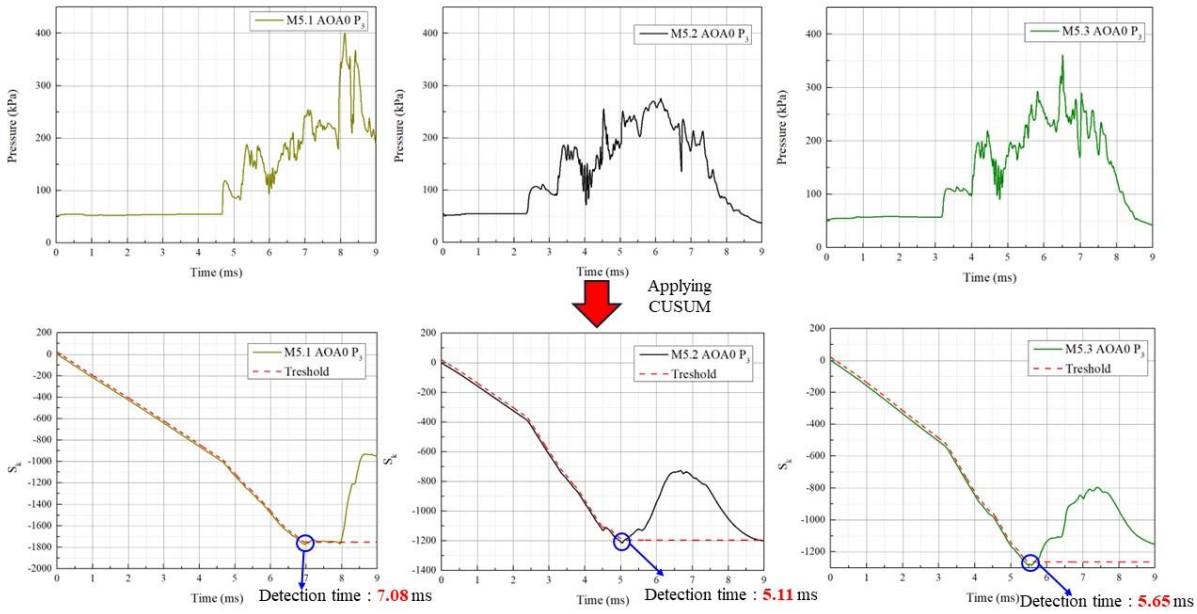

Fig 9. CUSUM algorithm for P3 sensor at angle of attack 0 degree

5. Conclusion

The unstart process induced by fuel injection is simulated using a two-dimensional Hybrid Mesh. The unstart is simulated by increasing the mass flow rate of injected fuel, and its adequacy is confirmed using the Korkegi criterion. To analyze the flow characteristics of unstart, pressure sensors are placed on the upper wall of the internal duct, and the arrival time of unstart is detected using the CUSUM algorithm. Additionally, variations in unstart characteristics with changes in Mach number and angle of attack are analyzed to understand the effect of flight conditions. It is observed that an increase in the angle of attack led to a delay in unstart, while variations in Mach number resulted in both delays and accelerations of unstart. Future research will focus on expanding the analysis domain to 3D to investigate the characteristics of unstart in reacting flow and analyze the effects of liquid fuel injection on unstart.

References

1. Norris, G.: X-51A Scramjet fails on a second attempt. Aviation Week. https://aviationweek.com/x-51a-scramjet-fails-second-attempt (1995). Accessed 16 June 2011
2. Mashio, S., Kurashina, K., Bamba, T., Okimoito, S., Kaji, S.: Unstart phenomenon due to thermal choke in scramjet module. 10th International Planes and Hypersonic Systems and Technologies Conference, AIAA 2001-1887, 1-7 (2001)
3. Wagner, J.L., Yuceil, K.B., Valdivia, A., Clemens, N.T., Dolling, D.S.: Experimental Investigation of Unstart in an Inlet/Isolator Model in Mach 5 Flow, AIAA journal. Vol. 47. No. 6, 1528-1542 (2009)
4. Do, H.R, Im, S.K., Mungal, M.G., Cappelli, M.A.: The influence of boundary layers on supersonic inlet flow unstart induced by mass injection. Exp Fluids. 51. Springer, 679-691 (2011)
5. Im, S.K., Baccarella, D., McGann, B., Liu, Q., Wermer, L., Do, H.R.: Unstart phenomena induced by mass addition and heat release in a model scramjet. Journal of Fluid Mechanics. Vol. 797. Cambridge, 604-629 (2016)

6. Baccarella, D., Liu, Q., McGann, B., Lee, T.H.: Isolator Shock Dynamics of Mass Injection-Induced Unstart in a Circular Model Scramjet. 23rd International Planes and Hypersonic Systems and Technologies Conference, AIAA 2020-2428, 1-11 (2020)
7. Korkegi, R.H.: Comparison of Shock-Induced Two-and Three-dimensional Incipient Turbulent Separation. AIAA journal. Vol. 13. No. 4., 534-535 (1975)
8. Frost, M. A., Gangurde, D. Y., Paull, A., Mee, D. J.: Boundary-Layer Separation Due to Combustion-Induced Pressure Rise in a Supersonic Flow. AIAA Journal. Vol. 47. No. 4, 1050-1053 (2009)
9. Trapier, S., Deck, S., Deveau, P., Sagaut, P.: Time-frequency Analysis and Detection of Supersonic Inlet Buzz. AIAA journal. Vol. 45, No. 9, 2273-2284 (2007)
10. Hutchins, K.E., Akella, M.R., Clemens, N.T., Donbar, J.M.: Detection and Transient Dynamics Modeling of Experimental Hypersonic Inlet Unstart. 6th AIAA Flow Control Conference, 1-18 (2012)
11. Menter, F.R., Kuntz, M., Langtry, R.: Ten Years of Industrial Experience with the SST Turbulence model. Turbulence. Heat and Mass Transfer 4. 1-8 (2003)
12. Wilcox, D.C.: Turbulence Modeling for CFD. DCW Industry. California. 171-203 (2002)
13. Peng, S.H., Davidson, L., Holmberg, S.: A modified Low-Reynolds number K-W model for Recirculating Flows. Journal of Fluids Mechanics. Vol. 119. 867-875 (1997)
14. Gritskevich, M.S., Garbaruk, A.V., Schutze, J., Menter, F.R.: Development of DDES and IDDES Formulations for the k-w Shear Stress Transport Model. Flow Turbulence Combust. 867-875 (2012)
15. Cong, T.H., Park, W. G.: Evaluation of a new scaling term in Preconditioning schemes for computations of compressible cavitating and ventilated flows. Ocean Engineering 126. 432-466 (2016)
16. Kitamura, K., Hashimoto, A.: Reduced dissipation AUSM-family fluxes: HR-SLAU2 and HR-AUSM+-up for high resolution unsteady flow simulations. Computer and Fluids. Vol. 126. 41-57 (2016)
17. Moukalled, F., Mangani, L., Darwish, M.: The Finite Volume Method in Computational Fluid Dynamics. Springer. Switzerland. 241-244 (2015)
18. Park, J.S., Kim, J.A.: Higher-Order Discontinuous Galerkin-MLP Method on Triangular and Tetrahedral Grids. 20th AIAA Computational Fluid Dynamics conference. AIAA 2011-3059. 1-18 (2011)
19. Kim, H.W., Sung, H.G.: Numerical study on detection and quantification of scramjet engine unstart. 25th AIAA International Planes and Hypersonic Systems and Technologies Conference. AIAA. 1-12 (2023)